Preparation and Characterization of Titanium Dioxide Core/Polymer Shell Hybrid Composite Particles Prepared by Emulsion Polymerization

Dong-Guk Yu,[1] Jeong Ho An,[1] Jin Young Bae,[1] Yong Eui Lee,[2] Seong Deok Ahn,[2] Seung-Youl Kang,[2] Kyung Soo Suh[2]

[1]*Departmen of Polymer Science and Engineering, SKKU, Su-Won, 440-746, Korea*
[2]*Basic Research Laboratory, ETRI, 161 Gajeong-dong, Yuseong-gu, Daejeon, 305-350, Korea*

Received 30 May 2003; accepted 22 January 2004

ABSTRACT: Titanium dioxide inorganic core and polymer shell composite poly(methyl methacrylate-*co*-butylacrylate-*co*-methacrylic acid) [P(MMA-*co*-BA)-MAA] particles were prepared by emulsion copolymerization. Fourier transform IR (FTIR) spectroscopy was used to measure the content of MAA composite particles. Dynamic light scattering (DLS) characterized the composite particle size and size distribution. The field emission SEM (FE-SEM) results of the composite particles showed regular spherical shape and no bare TiO_2 was detected on the whole surface of the samples. The composite particles were produced, showing good spectral reflectance compared with bare TiO_2. TGA results indicated the encapsulation efficiency and estimated density of composite particles. Encapsulation efficiency was up to 78.9% and the density ranged from 1.76 to 1.94 g/cm^3. Estimated density of the composite particles is suitable to 1.73 g/cm^3, due to density matching with suspending media. © 2004 Wiley Periodicals, Inc. J Appl Polym Sci 92: 2970–2975, 2004

Key words: inorganic core; polymer shell; composite particles; emulsion polymerization; encapsulation efficiency

INTRODUCTION

Encapsulated particles consisting of an inorganic core and a polymer shell are of interest in various applications, such as cosmetics, inks, and paints, because of their better mechanical properties and dispersion stability of the suspension medium.[1–5] Polymers are encapsulated with inorganic particles; enhanced physical properties are to be expected.[6–9] It is, however, a common drawback that the inorganic particles heavily aggregate into clusters. Some approaches were made, aiming at this goal. When surfactants are used to modify the inorganic particles, the final products may be latently unstable because of phase separation of the surfactant. Above all, the enhancement in dispersion stability of hybrid composite particle is the most significant characteristic of inorganic core/polymer shell composite particles. The dispersion stability of hybrid composite particles themselves is determined by the contribution of three main factors: van der Waals attractive forces, electrostatic forces, and steric repulsive forces between particles. Derjaguin-Land au-Verwey-Overbeek (DLVO) theory is that the summation of attractive van der Waals forces and the electrostatic repulsion forces as a function of the interparticle distance results in a free energy of maximum that functions as a barrier and keeps the particles apart. If the particles have a large surface potential energy, they are stable enough to be stored for a relatively long time. Ionic strength and pH affects the particle surface potential energy. Polymer shell especially imparts the dispersion stability by the steric or electrostatic mechanisms.[10–13] Steric stabilization results from nonionizable polymer chains on the particle surface. If two particles approach each other, the polymer chains or segments that extend into the dispersion begin to overlap and hinder the attachment of the particles. Electrostatic stabilization by ionizable functional group, such as carboxylic acid, hydroxyl, amine, and sulfate, involves both electrostatic and steric mechanisms.

In this study, poly(methyl methacrylate-*co*-butylacrylate-*co*-methacrylic acid) [P(MMA-*co*-BA)-MMA] shell composite particles were prepared with emulsion polymerization of methyl methacrylate (MMA), *n*-butylacrylate (*n*-BA), and methacrylic acid (MAA). Occasionally, the inorganic/organic composite particles were produced by coupling already existing polymer chains to the organic surface or polymerizing in the interface of inorganic particles; dispersion stability of TiO_2 in monomer mixture is crucially dependent on the surface characteristics of TiO_2 in dispersion state

Correspondence to: D.-G. Yu (polyyoo@skku.edu).
Contract grant sponsor: Korea Ministry of Information and Communications.

TABLE I
Recipes for Emulsion Polymerization of TiO_2/P(MMA-*co*-BA)-MAA Composite

		Monomer			Surfactant			
Sample ID	TiO_2 (g)[a]	MMA (g)	BA (g)	MAA (g)	SLS (g)	Triton X-100 (g)	APS (mg)[b]	DI water (g)
TPMA[c]-5	4	6	0.6	0.3	0.125	0.25	69	400
TPMA-10	4	6	0.6	0.6	0.125	0.25	72	400
TPMA-15	4	6	0.6	0.9	0.125	0.25	75	400

[a] 1 wt % of reaction medium.
[b] 1 wt % of total monomer.
[c] TiO_2/P (MMA-*co*-BA)-MAA.

during polymerization. In this contribution, the usefulness of emulsion polymerization in producing a carboxylic acid functional group TiO_2/P(MMA-*co*-BA)-MAA hybrid composite particles was estimated by considering the surface characteristics of composite particles. Finally, their spectral intensity and density were estimated to find an appropriate application in electrophoretic displays.

EXPERIMENTAL

Materials

MMA and *n*-BA (Sigma-Aldrich Co. Ltd.) were chemically pure grade and purified by reduced pressure distillation. MAA was used as shipped. Ammonium persulfate (APS) was purified by recrystallization and sodium lauryl sulfate (SLS) and Triton X-100 of commercial product grade were used without further purification. Titanium dioxide (TiO_2 R-900, DuPont Ti-Pure) pigment particles with average particle size of 0.42 μm were used as core materials.

Polymerization procedure

Emusifiers (SLS and Triton X-100) and the inorganic TiO_2 dispersed mixed solvent were introduced into the reaction flask, heated to 70°C, and stirred at a rate of 250 rpm. The nitrogen gas was bubbled through the solution for deoxygenation. After 30 min, APS and the monomer mixture were poured into the reaction flask. The reaction was then allowed to polymerize for 24 h under the constant stirring rate. Cooling to room temperature terminated the reaction. Deionized water was added to the pigment/polymer composite particles mixture and mixed thoroughly. The pigment/polymer composite particles were isolated from the mixture by centrifugation. The supernatant was decanted and the remaining pigment/polymer composite particles were washed with deionized water five times. Finally, the pigment/polymer composite particles were dried at −90°C in a freeze drier. The representative recipe and the reaction parameters investigated in this study are shown in Table I. Here, TiO_2/P(MMA-BA)-MAA hybrid composite particles are symbolized by TiO_2/P[(MMA-co-BA)-MAA] (TPMA-α), where α is the percentage of weight fraction of MAA.

Characterization

A Fourier transform infrared spectrophotometer (FTIR) was used to characterize the functional groups of the pigment/polymer composite particles. The pigment/polymer composite sample was ground with dried potassium bromide (KBr) powder and compressed into a disc. The KBr disc was subjected to analysis by an IR spectrophotometer. The particle size and particle-size distribution were measured by dynamic light scattering (DLS, Brookhaven). The samples for DLS were prepared by dilution with methanol. The surface morphology was observed with a field-emission scanning electron microscope (FE-SEM, Hitachi S-4300). Powder XRD spectra patterns were obtained with a MAC Science M18 X-ray diffractometer (100 kV, 200 mA) with CuKα and Ni filter with a wavelength of 0.154 nm at a scanning rate of 3°/min. The 2θ ranged from 10° to 80°. Spectral reflectance measurement was made by using an integrating sphere arrangement (ISR-260, Shimadzu Science Instruments, Columbia, MD), and spectra were obtained over the wavelength range from 400 to 700 nm. The spectral reflectance of the samples was measured relative to a zinc oxide (ZnO) standard plate. To evaluate the thermal property, the coating efficiency, and the density of the inorganic/polymer hybrid composite particles, thermal analysis was done for the powder of the composite materials obtained from a freeze drier for 3 days. Samples of 10–30 mg powder were put into an Au crucible for TGA. The heating rate was 10°C/min in nitrogen gas. The recorded temperature range was from 50 to 650°C. The experimental encapsulation efficiency of TiO_2 (E_{TiO2}) and experimental density of composite particles were determined by incineration of the polymer shell by using a TGA. The percentage of TiO_2 encapsulation efficiency was calculated as

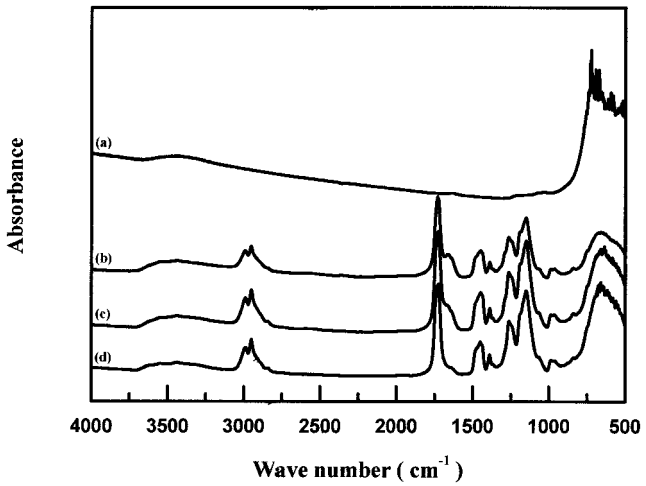

Figure 1 FTIR spectra of (a) bare TiO_2, (b) TPMA-5, (c) TPMA-10, and (d) TPMA-15.

$$E_{TiO_2} = (\text{residual weight of } TiO_2 \text{ after incineration})/(\text{theoretical weight of } TiO_2 \text{ in samples}) \times 100 \quad (1)$$

where theoretical weight of TiO_2 is defined as

$$\text{Theoretical weight of } TiO_2 = (\text{weight of dried sample}) \times (\text{weight fraction of } TiO_2 \text{ in the sample}) \quad (2)$$

$$\text{Theoretical weight fraction of } TiO_2 = (\text{weight of } TiO_2)/(\text{weight of polymer} + \text{weight of } TiO_2) \quad (3)$$

$$\text{Density (g/cm}^3) = 4.1 \times (\text{weight fraction of } TiO_2 \text{ in dried sample}) + 1.1 \times (\text{weight fraction of polymer}) \quad (4)$$

RESULTS AND DISCUSSION

FTIR spectroscopy results for the samples are shown in Figure 1. Figure 1(a) corresponds to the TiO_2 raw material and Figure 1(b–d) corresponds to the TPMA-5, TPMA-10, and TPMA-15 composite particles. Figure 1(a) shows the spectrum of bare TiO_2 particles. The vibration absorption at low frequencies, such as at 800 cm^{-1}, shows the existence of a Ti—O—Ti backbone. The region around 3400–3600 cm^{-1} has characteristic peaks for hydroxyls on TiO_2 particle surface. In the spectrum of Figure 1(c–d) samples, it is observed that the functional group through the presence of bands region 1680–1730 cm^{-1} belongs to C═O asymmetric and symmetric vibrations of the carboxylic acid. The bands at 1236 and 1100 cm^{-1} are attributed to the vibration of the C—O—C bands, whose identification with FTIR spectroscopy was already described. In Figure 1(c, d), it is possible to observe a broad band region of 3300–3600 cm^{-1} associated with the hydroxyl groups. The band in the region 2800–3000 cm^{-1} corresponds to the CH_2 and CH_3 group of polymer backbone. The bands at 1730 cm^{-1} are assigned to symmetric C═O stretch of the carboxylic acid in the same results of reference. In addition, the region of bands 500–800 cm^{-1} is tentatively assigned to Ti—O—Ti groups. These above results of FTIR spectrum prove the formation of the composite particles.

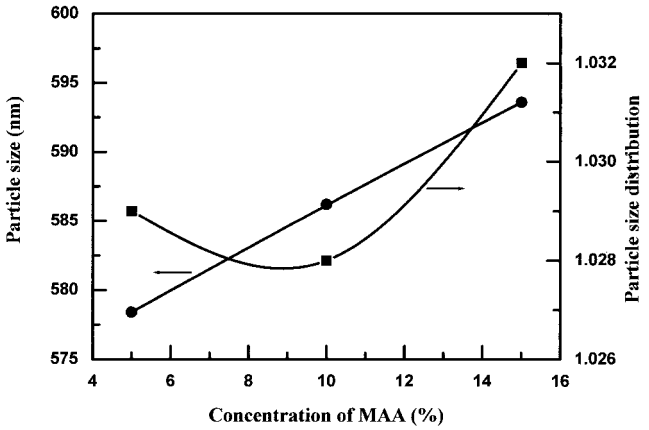

Figure 2 Mean particle size (●) and particle size distribution (■) of composite particles with the MAA concentration.

The particle size and particle-size distributions were determined as shown in Figure 2. The average particle diameters and weight particle diameters are summarized in Table II. In the case of the composite, particles were average particle size, ranging from 578.4 to 593.6 nm. The particle-size distribution observed narrow distributions in most cases, but is relatively narrower than bare TiO_2. There is no MAA in the reaction in the early nucleation stage when MAA was added in the

TABLE II
Particle Size and Size Distribution of Bare TiO_2 and TiO_2/P(MMA-*co*-BA)- MAA Composite

Sample ID	Particle size (nm)		PDI
	D_n[a]	D_w[b]	(D_w/D_n)
TiO_2[c]	425.5	462.5	1.087
TPMA-5	578.4	595.2	1.029
TPMA-10	586.2	602.6	1.028
TPMA-15	593.6	612.6	1.032

[a] Number-average diameter.
[b] Weight-average diameter.
[c] Bare TiO_2.

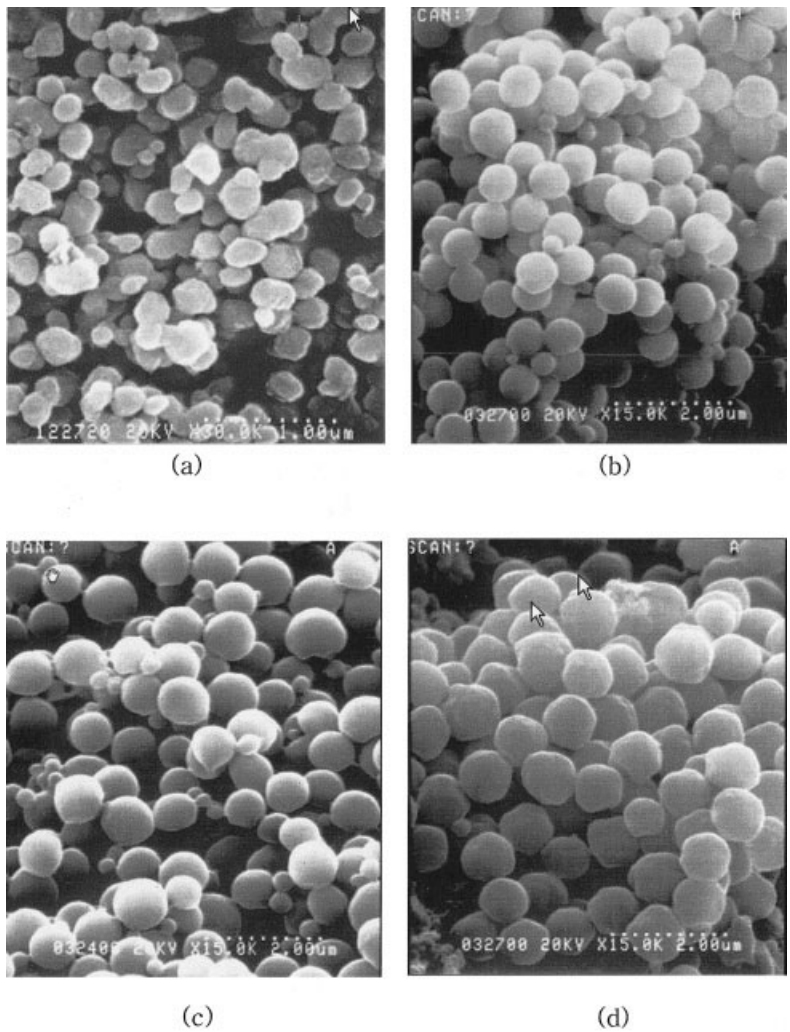

Figure 3 FE-SEM micrographs of (a) bare TiO_2, (b) TPMA-5, (c) TPMA-10, and (d) TPMA-15.

latter nucleation stage. Therefore, a large amount of flocculation occurred between the primary particles at the beginning of the nucleation because of the absence of carboxylic acid located at the surface. As a result, the average particle diameter of the TPMA-15 is larger than TPMA-5. MAA is mainly located at the surface of the composite particles, so average particle diameter increases with increasing concentration of MAA.

Figure 3(a) shows an FE-SEM image of bare TiO_2 particles. Particles exhibit an irregular spherical shape heterogeneously distributed, which is characteristic of conventional TiO_2 particles usually obtained. When bare TiO_2 particles are introduced in the polymerization medium, investigation of the morphology of the resulting composite particles by FE-SEM reveals that small pure TiO_2 particles are covered with polymer. This is seen in Figure 3(b–d). From this observation, one can deduce that the bare TiO_2 particles are either encapsulated during the polymerization or embedded in the polymer or more anchored in the polymer. The surface of the composite particles was smooth and regularly spherical shaped and no bare TiO_2 particle was detected on the whole surface of the samples.

Figure 4 contains the XRD patterns of bare TiO_2 and TPMA-α composite particles. In Figure 4(a), bare TiO_2 diffraction patterns reveal three main peaks: 2θ values of 27°, 36°, and 43° correspond to the rutile TiO_2. In Figure 4(b–d), the broad peak between 15° and 25° is assigned to amorphous polymer and the three peaks appear rutile TiO_2.

The spectral reflectance of ZnO, bare TiO_2, and composite samples are shown in Figure 5. Compared with the bare TiO_2, all the composite samples displayed slightly low spectral reflectance. This happens because the polymer shell of the composite samples protected the penetration of UV. However, polymer shell thickness is about 200 nm, and UV light penetrates the polymer shell. Thus, all the composite samples show nearly the same as bare TiO_2 spectral reflectance.

Figures 6 and 7 show the TGA thermograms obtained from the bare TiO_2, P(MMA-*co*-BA)-MAA reference, and composite samples. Obviously, the onset

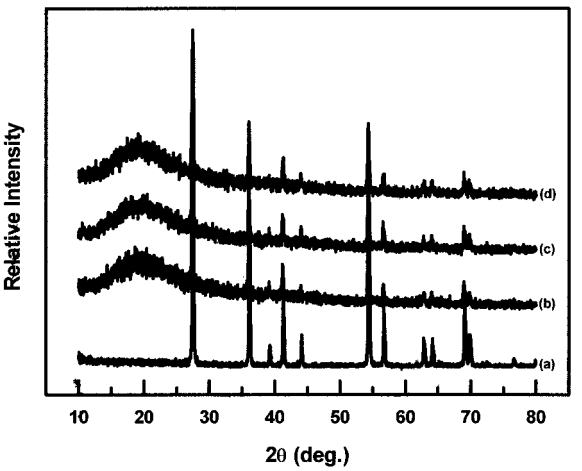

Figure 4 X-ray diffractograms of (a) bare TiO_2, (b) TPMA-5, (c) TPMA-10, and (d) TPMA-15.

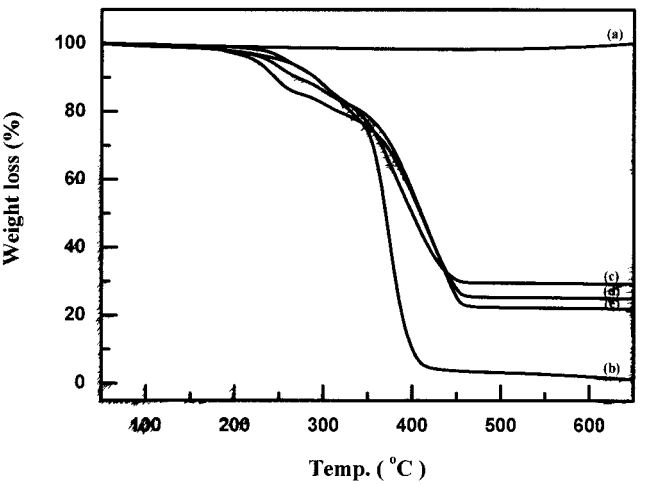

Figure 6 TGA thermograms of (a) bare TiO_2, (b) P(MMA-*co*-BA) reference, (c) TPMA-5, (d) TPMA-10, and (e) TPMA-15.

temperature of thermal decomposition shown by those composites [Fig. 7(b–(d)] was shifted toward the higher temperature range than that of reference polymer [Fig. 7(a)], indicating the enhancement of the thermal stability of the composite samples. It is noticeable that the composites show the onset temperature at a range of 386.8, 410.1, and 408°C of their polymer content increase, respectively. Table III also provides the encapsulation efficiency and estimated density of the TPMA-α composite samples. In general, the encapsulation efficiency depended on the ratio of core materials, TiO_2 : polymer shell polymer. In this, TPMA-α was used as the encapsulating polymer (TPMA-5, TPMA-10, TPMA-15, the TiO_2 to TPMA-α ratio = 1 : 1.725, 1.8, 1.875), and the encapsulation efficiency ranged from 61.7 to 78.9% of TiO_2 in the oil phase being encapsulated. The encapsulation efficiency was decreased with increasing concentration of MAA. Also, the estimated density was decreased with increasing concentration of MAA. The density of the composite samples ranged from 1.76 to 1.94g/cm^3. The estimated density was lower than that of the theoretical density. The lower encapsulation efficiency and estimated density of the higher concentration of MAA probably resulted from the escape of TiO_2 particles entrapped inside the droplets into continuous phase.

CONCLUSION

TiO_2 core and P(MMA-*co*-BA)-MAA shell hybrid composite particles are successfully prepared by emulsion

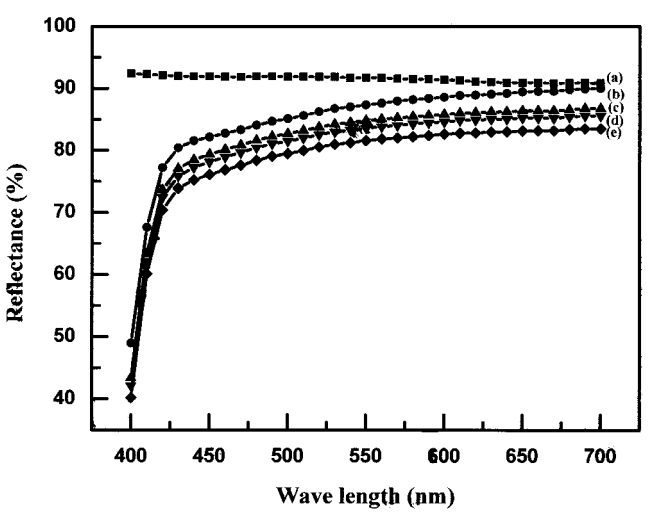

Figure 5 Spectral reflectance of (a) ZnO standard, (b) bare TiO_2, (c) TPMA-5, (d) TPMA-10, and (e) TPMA-15.

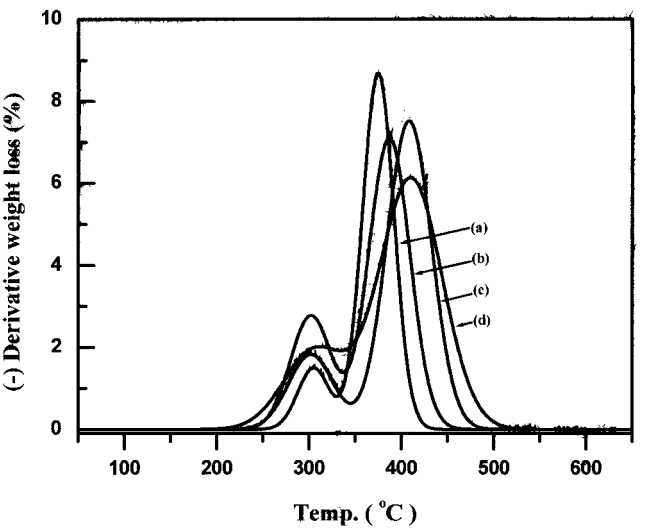

Figure 7 Derivative weight loss of (a) P(MMA-*co*-BA) reference, (b) TPMA-5, (c) TPMA-10, and (d) TPMA-15.

TABLE III
TGA Thermograms, Encapsulation Efficiency, and Density of TMA- Composite Samples

Sample ID	Weight (mg)		Decomposed onset temp.[a] (°C)	Encapsulation efficiency (%)	Estimated density (g/cm^3)	Theoretical density (g/cm^3)
	Initial	Final				
TiO_2	20.32	20.38	—	—	—	4.1
Polymer[b]	20.85	0.17	374.7	—	—	1.06[c]
TPMA-5	14.48	4.19	386.8	78.9	1.94	2.21
TPMA-10	15.63	3.91	410.1	70.0	1.82	2.18
TPMA-15	13.85	3.05	408.1	61.7	1.76	2.15

[a] Main maximum decomposition temperature.
[b] P(MMA-*co*-BA).
[c] Density of PMMA.

polymerization. The presence of carboxylic acid groups on the composite particles was confirmed by FTIR. A DLS and FE-SEM result of the composite particles was narrow size distribution and regular spherical shape and no bare TiO_2 particle was detected on the whole surface of the samples, respectively. XRD patterns of the broad band reflected amorphous polymer composite. The UV results show that the decrease in the spectral reflectance values was negligibly small; it is believe that the composite samples would not cause any problem in the ultimate usage. The TGA results indicated the encapsulation efficiency and density of composite particles. Encapsulation efficiency was up to 78.9% and estimated density range was from 1.76 to 1.94 g/cm^3. The estimated density of the composite TiO_2 particles is suitable to 1.73 g/cm^3, due to density matching with suspending media. It is concluded that in producing inorganic/polymer composite particles. In further applications, they are expected to find great usefulness in electrophoretic displays.

The Korea Ministry of Information and Communications financially supported this work.

References

1. Haga, Y.; Inoue, S.; Sato, T.; Yosomiya, R. Angew Makromol Chem 1986, 139, 49.
2. Caris, C. H. M.; Herk, A. M.; Louissa, P. M.; German, A. L. Br Polym J 1989, 21, 133.
3. Hasegawa, M.; Arai, K.; Saito, S. J Polym Sci, Part A: Polym Chem 1987, 25, 3231.
4. Caris, C. H. M.; Kuijpers, R. P. M.; Heck, A. M.; German, A. C. Makromol Symp 1990, 35, 335.
5. Erdem, B.; Sudol, E.; Dimonie, V. L.; El-Aasser, M. S. J Polym Sci, Part A: Polym Chem 2000, 38, 4419.
6. Goyanes, S. N.; Marconi, J. D.; Konig, P. G.; Matteo, C. L.; Rubiolo, G. H.; Marzocca, A. J. Polymer 2001, 42, 5267.
7. Kawaguchi, H. Prog Polym Sci 2001, 25, 1171.
8. Chan, Y. N.; Craig, G. S. W.; Schrock, R. R.; Cohen, R. E. Chem Mater 1992, 4, 885.
9. Gupta, P. K.; Hung, T. C.; Lam, F. C.; Perrier, D. G. Int J Pharm 1998, 43, 167.
10. Castellanos, J. R.; Mendizabal, E.; Puig, J. E. J Appl Polym Sci, Appl Polym Symp 1991, 49, 91.
11. Mendizabal, E.; Castellanos-Ortega, J. R.; Puig, J. E. Colloids Surf 1992, 63, 209.
12. MacGregor, J. F.; Penlidis, A.; Hamielec, A. E. Polym Process Eng 1984, 2, 179.
13. Elicabe, G. E.; Meira, G. R. Polym Eng Sci 1988, 28, 121.